IDENTIFICATION OF WAVE TYPES, DIRECTIONS, AND VELOCITIES USING SMART-1 STRONG MOTION ARRAY DATA

C. H. Loh (I)
J. Penzien (II)
Presenting Author: C. H. Loh

SUMMARY

Presented in this paper is a method for identifying wave types, directions, and velocities contained in strong earthquake ground motions. After transforming the motions into components along their principal axes, use is made of a principal variance ratio R(f), defined as the ratio of the minor principal variance to the major principal variance for those components of motion within frequency band Δf centered on frequency f_o. At those frequencies where R(f) has very low values, single wave types dominate the motions. Using directions of principal axes and phase lag information, wave types, directions, and velocities are identified.

INTRODUCTION

At a meeting in Hawaii during May 1978, the need for strong earthquake ground motion arrays was discussed and plans were developed for promoting such arrays in many locations on a world-wide basis (Ref. 1). One site selected at the workshop as having high potential for frequently experiencing future strong motions was north-eastern Taiwan. Responding to the great need, a strong motion array was installed in this area in the town of Lotung in the fall of 1980 under the joint effort of the Academia Sinica in Taiwan and the versity of California, Berkeley, with financial support provided by the ional Science Council and the National Science Foundation (Ref. 2).

The strong-motion array in Lotung, called SMART-1, is a two-dimensional face array consisting of a center station C00 and three concentric circles ner I, middle M, and outer O) each having 12 stations with radii of 200 ers, 1 km, and 2 km, respectively, as shown in Fig. 1. This arrangement of stations was selected to optimize the expected information to be obtained m both the engineering and seismological points of view. The instruments this array record digitally with a common time base accurate to 1 millionond over a duration which includes 2.5 seconds of pre-trigger memory. tunately, many earthquakes have triggered the array since the installation viding a wealth of strong ground motion data.

It is the purpose of this paper to present selected results of a single dy carried out using SMART-1 data in which a promising method for identing wave types, directions, and velocities was developed. Due to space itations, application of the method herein is restricted to a limited ber of motions recorded during the earthquake of January 29, 1981 (Event 5);

) Associate Professor of Civil Engineering, National Central Universtiy, Taipei, Taiwan, China

) Professor of Structural Engineering, University of California, Berkeley, California, U.S.A.

see Ref. 2. This earthquake was centered 30 km S26°E of the center of the array. Its focal depth was 11 km and its Richter magnitude calculated locally by the Institute of Earth Sciences in Taipei was 6.9.

CROSS CORRELATIONS AND PRINCIPAL DIRECTIONS

In an attempt to identify wave types, directions, and velocities produced by the earthquake of January 29, 1981 (Event 5), let us first examine the cross correlation coefficient given by

$$\rho_{ij}(\tau) \equiv \frac{R_{ij}(\tau)}{\sqrt{R_{ii}(0)\ R_{jj}(0)}} \tag{1}$$

where

$$R_{ij}(\tau) \equiv \int_{t_o - \frac{\Delta T}{2}}^{t_o + \frac{\Delta T}{2}} x_i(t)\ x_j(t+\tau)\ dt \tag{2}$$

and where $x_i(t)$ and $x_j(t)$ are the recorded acceleration time-histories in the x-direction (East-West) at stations i and j, respectively; see Fig. 2. In Eq. (2), ΔT is a time window centered on time t_o, and τ is a time lag. If the ground motions at these stations were produced primarily by a single travelling wave, then the above cross correlation coefficient, which can range from +1 to -1, would show high correlation for τ equal to the time required for the wave to travel between the two stations. This value of τ would, of course, depend upon the direction of wave propagation as well as wave velocity.

Using t_o = 50.3 sec and ΔT = 7.0 sec so as to include the significant high intensity portions of the motions recorded at all stations in the time window of Eq. (2), cross correlation coefficients were generated over the range $0<\tau<3$ sec for many station pairs. It is pertinent to point out that the plots of these coefficients against time lag τ are not characteristic of those produced by pairs of motions dominated by a single travelling wave. Their shapes and low values of cross correlation suggest the simultaneous presence of multiple waves travelling in different directions with different velocities. Selecting the maximum cross correlation coefficient on each plot, one can examine the relationship between maximum cross correlation and distance (true distance; not projected distance) as shown in Fig. 3. In this figure, the exponential curve was derived by a least squares fitting of the data points shown. The rapid loss of maximum cross correlation with distance supports the above suggestion that multiple waves having different wave velocities and directions are simultaneously present at all stations. As a consequence of this observation, it was concluded that resolution of the motions into their frequency components and into their principal directions was required before identification of wave types, directions, and velocities could be made possible.

Following along these lines, let us transform the x and y recorded components of horizontal ground motion at a point into their $\tilde{x}$ and $\tilde{y}$ components in accordance with Fig. 2; thus,

$$\begin{aligned} \tilde{x}(t) &= x(t)\ \cos\phi + y(t)\ \sin\phi \\ \tilde{y}(t) &= -x(t)\ \sin\phi + y(t)\ \cos\phi \end{aligned} \tag{3}$$

Next, using time and frequency domain windows, the Fourier transforms of these new components are calculated using relations of the type

$$A_{\tilde{x}}(f) \equiv \int_{t_o - \frac{\Delta T}{2}}^{t_o + \frac{\Delta T}{2}} \tilde{x}(t) \exp(-i2\pi ft)dt \tag{4}$$

$$\tilde{x}(t) = \int_{-f_o - \frac{\Delta f}{2}}^{-f_o + \frac{\Delta f}{2}} A_{\tilde{x}}(f) \exp(i2\pi ft)\, df + \int_{f_o - \frac{\Delta f}{2}}^{f_o + \frac{\Delta f}{2}} A_{\tilde{x}}(f) \exp(i2\pi ft)\, df \tag{5}$$

where window lengths ΔT and Δf are centered on time t_o and frequency f_o, respectively.

The direction of maximum intensity as a function of frequency f_o can be obtained by maximizing the variance function

$$R_{\tilde{x}_i\tilde{x}_i}(\tau=0,\phi) = R_{x_ix_i}(0)\cos^2\phi + R_{y_iy_i}(0)\sin^2\phi + 2R_{x_iy_i}(0)\cos\phi\sin\phi \tag{6}$$

with respect to ϕ giving (Refs. 3,4,5)

$$\phi_o(f_o) = \frac{1}{2}\tan^{-1}\frac{2R_{x_iy_i}(0)}{R_{x_ix_i}(0) - R_{y_iy_i}(0)} \tag{7}$$

Angle $\phi_o(f_o)$ in Eq. (7) denotes two principal directions which are 90° apart; one being the major principal direction, the other the minor principal direction. The corresponding principal variances will be denoted by $R_{\tilde{x}_i\tilde{x}_i}(f_o)$ and $R_{\tilde{y}_i\tilde{y}_i}(f_o)$, respectively.

PRINCIPAL VARIANCE RATIO

Let us now define a principal variance ratio as given by

$$R(f_o) \equiv \frac{R_{\tilde{y}_i\tilde{y}_i}(f_o)}{R_{\tilde{x}_i\tilde{x}_i}(f_o)} \tag{8}$$

which varies over the range $0<R<1$. If we examine the motion at station i for discrete values of f_o, consistent with the discrete frequencies of the Fast Fourier Transform (FFT) method used in evaluating Eqs. (4) and (5), we find the following results: (1) When $R(f_o)=1$, there are no principal directions because the harmonic motion at frequency f_o moves along a circular path at constant angular velocity $2\pi f_o$ as shown in Fig. 4; i.e., the motion is equivalent to two resultant harmonics in orthogonal directions having equal amplitudes but being 90° out-of-phase, (2) When $0<R(f_o)<1$, principal directions do exist with the motion being along an ellipse; i.e., the motion is equivalent to two resultant harmonics in orthogonal directions with different amplitudes and they are 90° out-of-phase, and (3) When $R(f_o)=0$, principal directions exist but the motion is along a straight line; i.e., a pure harmonic exists. For $R(f_o)>0$, the two orthogonal waves could be made up of the superposition of multiple waves moving in different directions. Thus, in the interest of identifying wave types,

directions, and velocities, attention should be concentrated on those discrete frequencies having low values of $R(f_o)$. Fortunately for the SMART-1 data analyzed, these frequencies represent frequencies of high energy transmission as will be shown subsequently.

Figure 5 shows plots of the major principal variance $R_{\tilde{x}_i\tilde{x}_i}(f_o)$, the principal variance ratio $R(f_o)$, and the dominant (or major principal) direction $\phi_o(f_o)$ for the horizontal ground motions recorded at stations C00, I03, and I06. It is significant to note that at frequencies f_1, f_2, f_3, and f_4, representing high intensity motions, i.e., high major principal variances, the corresponding principal variance ratios are low indicating dominant wave transmissions in the neighborhood of these frequencies. Note that the dominant directions are nearly toward the epicenter for frequencies f_1 and f_2 but are much closer to the normal direction for frequencies f_3 and f_4. If the dominant waves are propagating in the general direction away from the epicenter, this observation suggests that Rayleigh waves are the primary source of energy transmission for frequencies less than about 2.5 Hz and that shear waves (SH waves; perhaps in part Love waves) are the primary source of energy transmission for frequencies from 2.5 Hz to about 6 Hz. Above these frequencies, the directions of propagation are quite variable.

Let us now examine in further detail the dominant directions of motions at frequencies $f_1 = 1.17$ Hz and $f_3 = 2.85$ Hz for many stations in addition to stations C00, I03, and I06 represented in Fig. 5. As suggested above, the dominant ground motions at these frequencies seem to be caused primarily by Rayleigh and shear (SH) waves, respectively. Figures 6 and 7 show the dominant direction at frequencies 1.17 Hz and 2.85 Hz, respectively, at many stations as given by Eq. (7). The average dominant direction ϕ_o over the array is also shown in these figures. Note that the average dominant direction in Fig. 6 is reasonable close to the epicentral direction while the average dominant direction in Fig. 7 is close to the normal direction.

We may now use these two average dominant directions to generate corresponding functions

$$R_{\tilde{x}_i\tilde{x}_j}(\tau) \equiv \int_{t_o - \frac{\Delta T}{2}}^{t_o + \frac{\Delta T}{2}} \tilde{x}_i(t)\, \tilde{x}_j(t+\tau)\, dt \qquad (9)$$

for ground motions recorded at many station pairs across the array. Noting the maximum cross correlation for each station pair over the entire range of τ and the corresponding relative distance between stations as projected on the average dominant axis, valuable plots can be obtained as shown in Fig. 8. Each data point represents a station pair. The upper plot in Fig. 8 is for f_o equal to 1.17 Hz while the lower plot is for f_o equal to 2.85 Hz. Straight lines fitted by least squares yield wave velocities (inverse values of the line slopes) equal to 2.4 km/sec and 5.3 km/sec for the Rayleigh and shear wave velocities, respectively.

Because a uniform elastic half space transmits Rayleigh waves at a velocity equal to 0.9 times the shear wave velocity, an explanation is needed of the mixture in the same time window of SH waves with local velocity of 5.3 km/sec and Rayleigh waves with velocities of 2.4 km/sec. The usual seismological interpretation of this large difference in local apparent velocities is that

the SH waves are associated with longer travel paths from the earthquake source to the array in the vicinity of which the SH wave fronts move steeply upwards through the soil. Thus, the apparent shear wave velocity is largely controlled by the more rigid, deeper rocks in the crust. On the other hand, the Rayleigh waves develop near the surface between the source and the array so that their wave velocities are largely controlled by the shallower less stiff materials.

According to this explanation the vertical components of ground motion in the time window studied should be significant in the frequency range of the Rayleigh waves but relatively insignificant in the frequency range of the transverse shear waves described above. This prediction was tested by computing the three-dimensional particle motions as a function of frequency f_o. The results show that the particle orbits agree well with the above prediction; i.e., significant vertical displacements are present in the frequency band 0.25 to 1.5 Hz, but relatively small vertical displacements are present in the frequency band 2.5 - 3.1 Hz.

CONCLUDING STATEMENT

Although further verification is needed, the method presented herein for identifying wave types, directions, and velocities making use of major principal variances and directions and a principal variance ratio shows considerable promise. Since generating the above results, the authors have generalized the method to a consistent three-dimensional form which permits further improvement of the results.

ACKNOWLEDGMENTS

The authors express their sincere thanks and appreciation to the National Science Council and the National Science Foundation for their financial support of the SMART-1 array project through grants Nos. CEE-7908982 and 70-0202-M0001-03, respectively.

REFERENCES

1. Iwan, W. D. (Editor), Proc. Int. Workshop Strong Motion Earthquake Instrument Arrays, Hawaii, 103 (1978).

2. Bolt, B. A., Loh, C. H., Penzien, J., Tsai, Y. B., and Yeh, Y. T., "Preliminary Report On The SMART-1 Strong Motion Array In Taiwan," Earthquake Engineering Research Center Report UCB/EERC-82/13, University of California, Berkeley, (1982).

3. Penzien, J. and Watabe, M., "Characteristics of 3-Dimensional Earthquake Ground Motion," Earthquake Eng. Struct. Dynamics, 3, 365-373, (1975).

4. Kubo, T. and Penzien, J., "Analysis of Three-Dimensional Strong Earthquake Ground Motions Along Principal Axes, San Fernando Earthquake," Earthquake Eng. Struct. Dynamics, 7, 265-278, (1979).

5. Kubo, T. and Penzien, J., "Simulation of Three-Dimensional Strong Ground Motions Along Principal Axes, San Fernando Earthquake," Earthquake Eng. Struct. Dynamics, 7, 279-294, (1979).

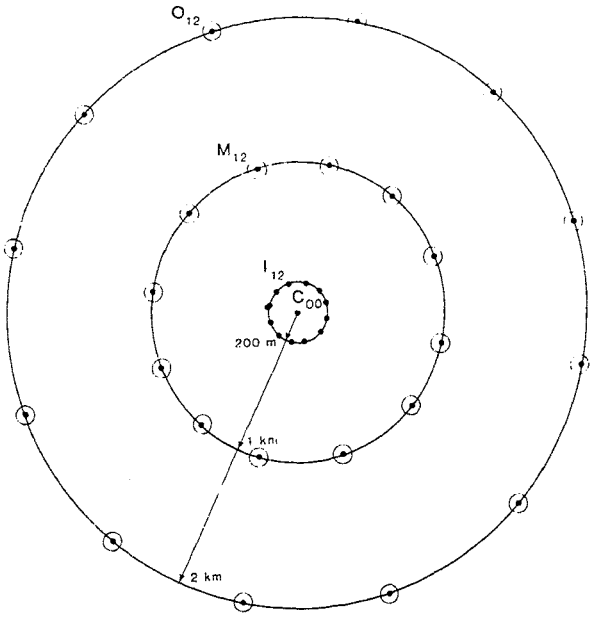

Fig. 1 The SMART 1 array

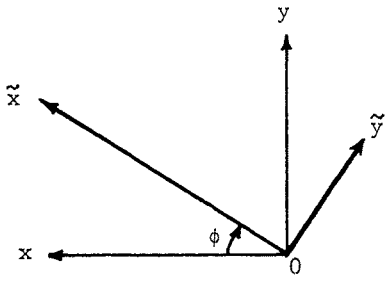

Fig. 2 Coordinate transformation of two horizontal components

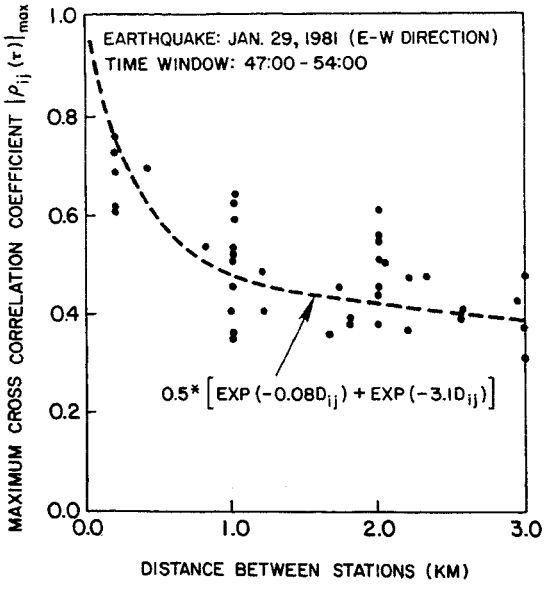

Fig. 3 Attenuation of correlation coefficient ρ

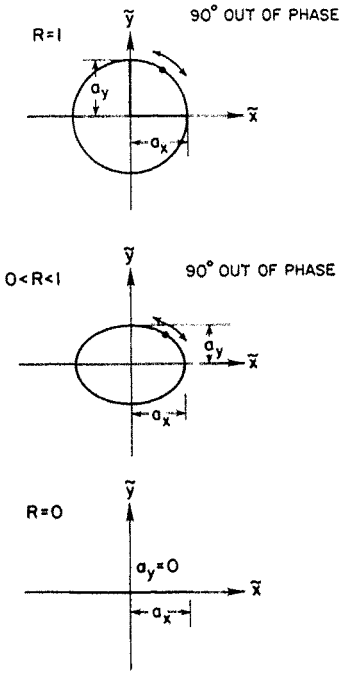

Fig. 4 Physical meaning of principal variance ratio

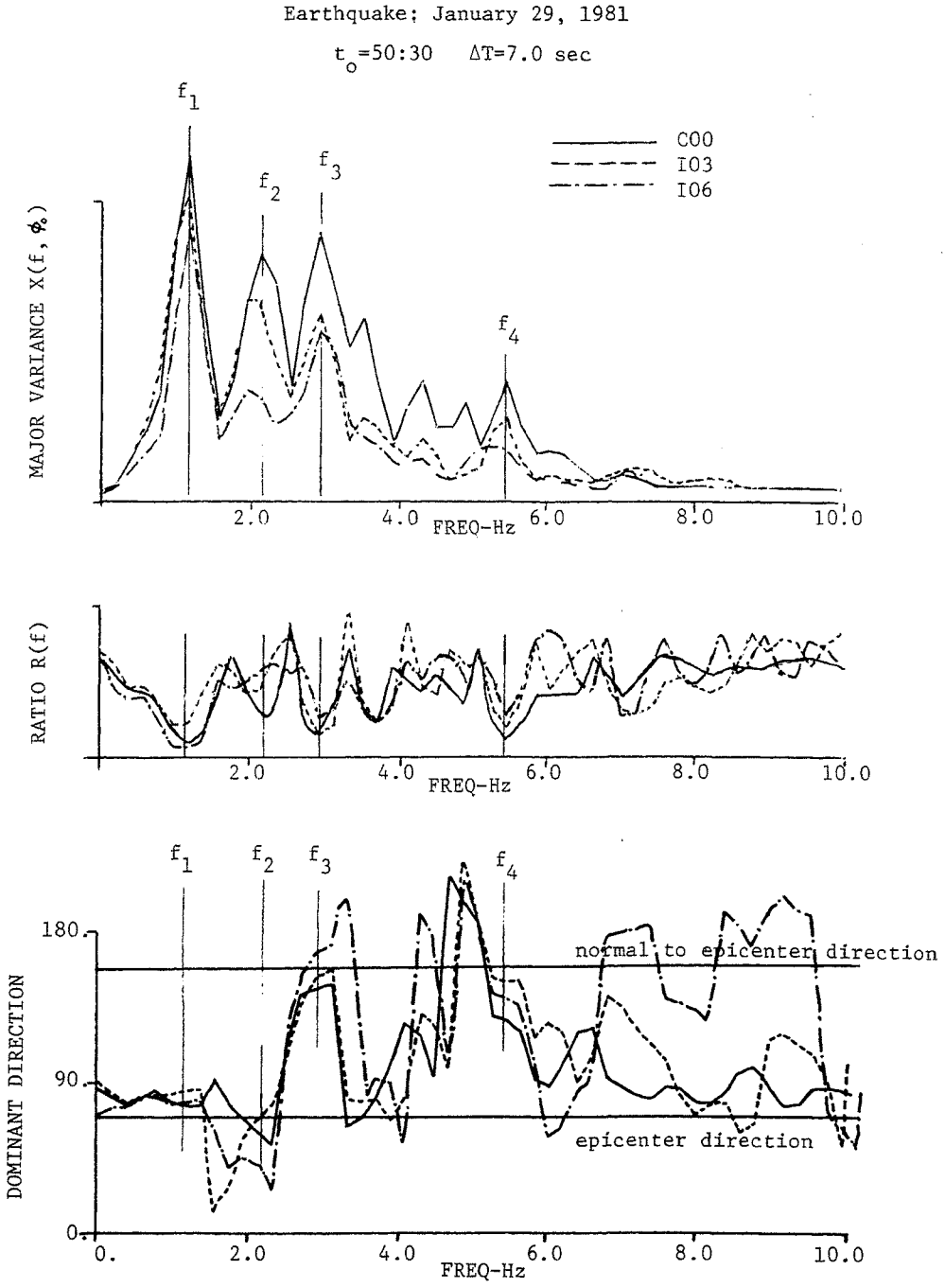

Fig. 5 Major principal variance, variance ratio and dominant direction for Event 5

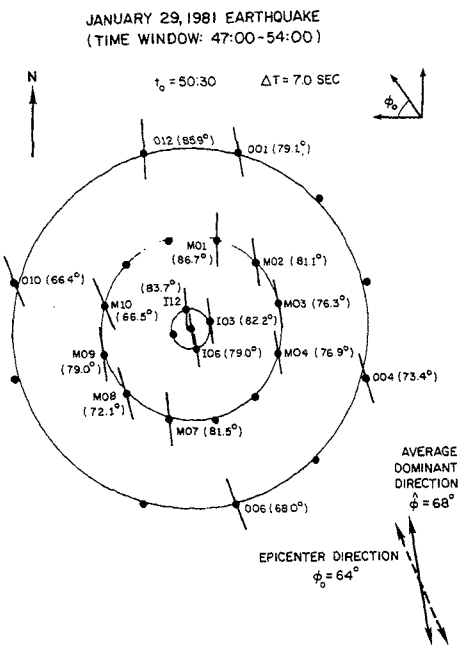

Fig. 6 Dominant directions at 1.17 Hz for Event 5

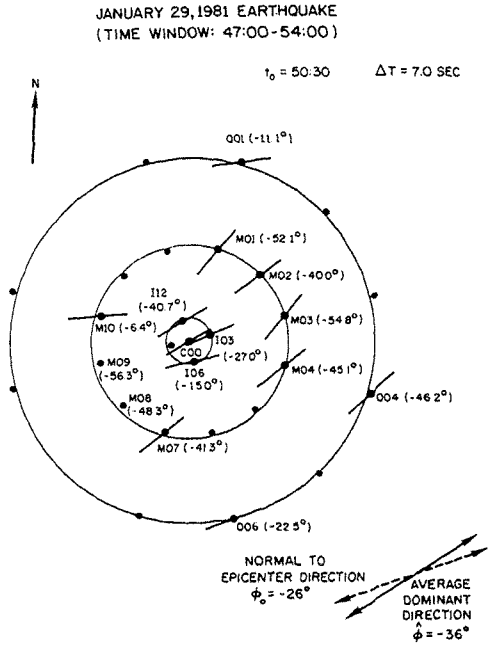

Fig. 7 Dominant directions at 2.85 Hz for Event 5

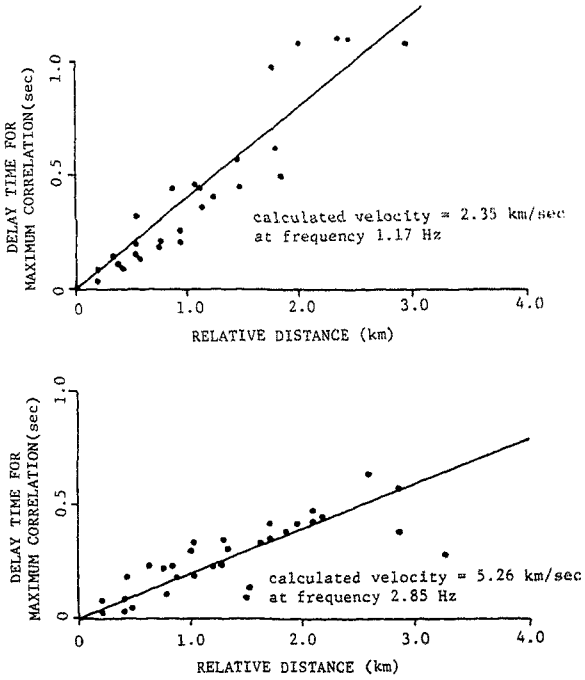

Fig. 8 Identification of wave velocity at frequencies 1.17 Hz and 2.85 Hz